

INSTRUMENT CAPABILITIES OF THE HP3 PERMITTIVITY PROBE

A. Stiegler⁽¹⁾, G. Kargl⁽¹⁾, and the HP³ instrument team

⁽¹⁾ Space Research Institute of the Austrian Academy of Sciences, Email: alexander.stiegler@oeaw.ac.at

ABSTRACT

In this work the capabilities of a bore-hole type Permittivity Probe (PP), originally developed for the ExoMars/Humboldt Station are presented. With this instrument electrical soil properties are derived as well as texture parameters like e.g. stratification or even density estimations. In this perspective a large number of laboratory measurements, testing the ability of the PP-instrument were performed. An extract of the obtained results including the detection of local inhomogeneities and the instrument-sensitivity to local water-abundances is presented here.

1. INTRODUCTION

As a part of the HP³ sensor suite the HP³-PP instrument was initially intended to be flown onboard the ExoMars Humboldt surface station. After the cancellation of the station it was decided to develop the Permittivity Probe further, until a laboratory model with a high proto-flight maturity level was achieved. The PP-instrument approach follows the concept of a classical Wenner array [1] which is shown in Fig. 1.

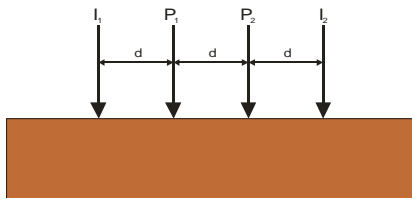


Fig. 1. The concept of a Wenner array type A.

Two transmitting electrodes $I_{1,2}$ project an alternating electrical field in the investigated material. Another two electrodes $P_{1,2}$ detect the transmitted signal which is influenced by the adjacent medium. In determining the local amplitude and phase variations to the injected signal the relative permittivity ϵ_r and the conductivity σ are determined following the equations [2]:

$$\epsilon_r = \frac{A_0}{A} \cdot \cos(\varphi - \varphi_0) \quad (1)$$

$$\sigma = \frac{A_0}{A} \cdot \omega \cdot \epsilon_0 \cdot \sin(\varphi - \varphi_0) \quad (2)$$

with A as the measured amplitude and φ as phase in the material respectively, with index 0 in vacuum. ϵ_0 is the vacuum permittivity and ω the angular frequency of the injected signal. In general the physical quantities permittivity and conductivity are defined as complex numbers. Considering the real and imaginary components of permittivity the dielectric loss tangent δ is defined as:

$$\tan(\delta) = \frac{\epsilon''}{\epsilon'} \quad (3)$$

The effective depth of investigation z_e for a Wenner array type A with electrode distance d , is defined as [3]:

$$\frac{z_e}{d} = 0.519 \quad (4)$$

Thus the possible depth to be explored is mainly dependent of the electrode configuration.

Further analysis of the calculated effective resistivities ρ_e - in the sense of solving an inversion problem - reveals textural parameters of the medium (e.g. stratification and local inhomogeneities) (see e.g. [4]).

As the measured effective permittivity and conductivity respectively, is a combination of every component in the investigated region, it is even possible to gain additional density and humidity information. An empirical formula for the connection between permittivity and bulk density was derived by Olhoeft and Strangway (1975) [5] for the moon. E.g. Topp's relation (1980) and Archie's law (1942) (summarized in [6]) give an estimation of the ambient water content in a sample. Theories of general mixing formulas for heterogeneous media are listed e.g. in [6] or [7].

2. THE INSTRUMENT

Permittivity Probe sensors for planetary space missions were proposed already for twenty years [8]. With the Permittivity Probes on Huygens and Philae two of them were selected to explore the electrical properties of their targets. [9, 10]. Selected for the ExoMars/Humboldt Station the HP³-PP sensor would have been the first permittivity instrument which is fully integrated on one mole. It was built as a follow up development of an ESA prototype [2]. Since it was initially planned to be located on a mole penetrator, the sensor was designed to be small and lightweight. The characteristic parameters of PP are listed in Tab. 1. An image of the PP-sensor mounted on the payload compartment is shown in Fig. 2.

Table 1. PP mole characteristics

parameter	value
length	250 mm
diameter	24 mm
mass front end electronics	15 g
electrode separation	42 mm
electrode area	30 * 35.121 mm ²
frequency range	4 – 20,000 Hz
frequency resolution	1 Hz
measurement error (uncalibrated)	<10 %
sampling rate	1 c/s
mean power consumption	166.1 mW

For technical reasons the payload compartment of HP³ was split into two half shells, containing the payload and mole electronics. The PP electronics consist of two redundant electronic boards operating each on one side of the payload compartment as a vector analyzer. Each electronic board is directly connected with the PP-electrode foils on the outer side of the payload compartment (Fig. 2). Each foil consists of two transmitting electrodes on the upper part, two receiving electrodes in the middle and one ground electrode at the end of the compartment. The resulting four transmitting electrodes (two for each foil) are equidistantly spaced around the cylinder.



Fig. 2. The PP-sensor with its electrode foils around the payload compartment.

Each transmitter patch is working independently of the others and all in all ten different transmitting configurations can be chosen. By switching various configurations the instrument is able to perform a virtual rotation without any mechanical movement. Thereby a 360° scanning of the surrounding medium is achieved. Following Eq. (4) for PP the effective depth of investigation is about 2.2 cm.

The nominal working frequency is in the range of 4 – 20000 Hz with a resolution of 1 Hz and a sampling rate of 1count/s independent of frequency.

With modifications of the electronic components frequencies up to 100 kHz could be achieved without changing the size and basic design of the breadboard. The evaluated permittivity value has an error of less than 10%. After the final calibration an error of approx. < 5% will be achieved.

3. INSTRUMENT CAPABILITIES

3.1 Scientific requirements

The scientific requirements of the permittivity sensor were determined to be:

- Determination of permittivity and conductivity of the regolith as a function of depth
- Revelation of the subsurface stratigraphy along the penetration path
- Determination of ice/water content of the regolith as a function of depth

In this perspective a vast amount of laboratory investigations with the PP model were performed to test the capabilities of the sensor.

3.2 Test results

The following laboratory test results are a selected quantity of measurements to demonstrate the capabilities of the HP³-PP sensor.

For calibration, physically stable polymers are used as reference samples. In Fig. 3 the relative permittivity signal of poly-methyl methacrylat (PMMA) is plotted versus frequency in comparison to values from Adiyodi et. al. (2009) [11]. The small deviation (less than 10 %) is expected as a result of chemical differences of the used materials, due to the production process.

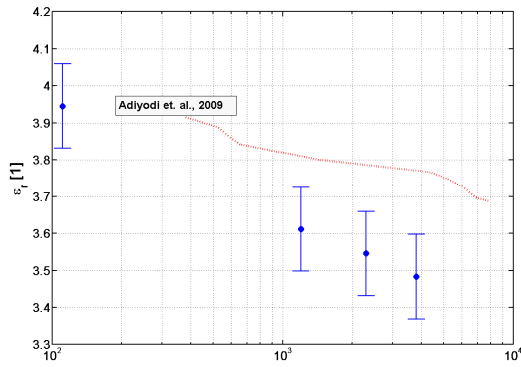


Fig 3. Relative Permittivity ϵ_r of a PMMA sample compared with Adiyodi et al.(2009) [11]

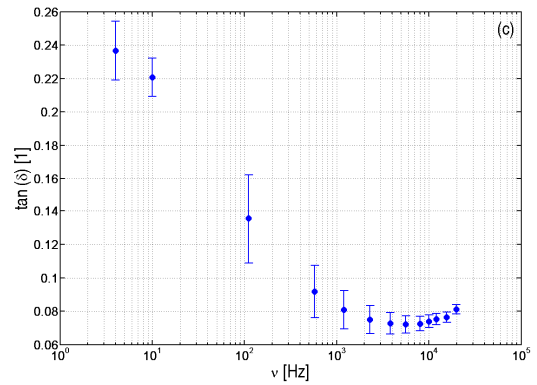
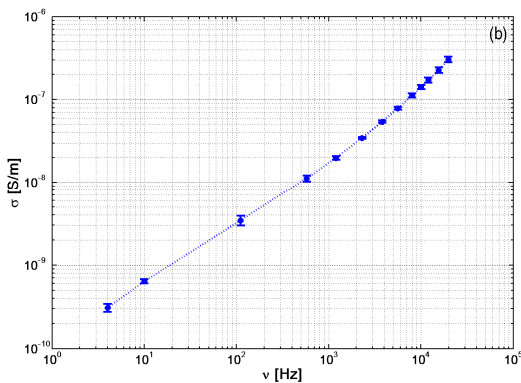
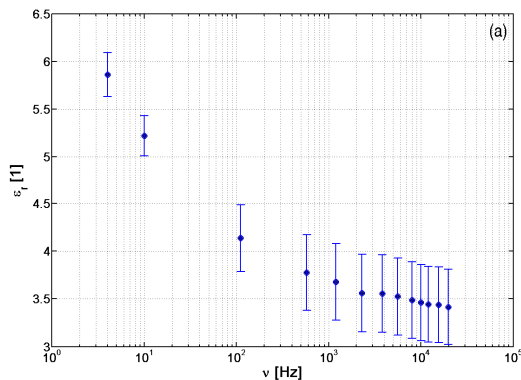


Fig 4. (a) Permittivity ϵ_r , (b) Conductivity σ and (c) dielectric loss tangent δ of a granular granite sample with maximum grain diameter of 3mm as function of frequency.

Fig. 4 contains the evaluated relative permittivity ϵ_r (a), conductivity σ (b) and dielectric loss tangent δ (c) of a granular granite sample with maximum grain diameter of 3mm versus the PP operation frequency. Notice the logarithmic scale of conductivity. With consideration that the electric properties are influenced by the formation process of the natural stone these values are in comparable agreement with common literature values (e.g. [12]).



In Fig. 5 the measured relative permittivity of the Martian soil analogue material Salten Skov is plotted as function of frequency. The presented data contains only relative permittivity values for frequencies beyond 1200 Hz. Below this frequency the permittivity values are strongly influenced by the ambient humidity, which consequently increases the evaluated value to more than 100% of the expected range. As a general feature all small grained materials exhibit a strong hygroscopic behaviour, making it difficult to separate between material permittivity and the bulk value containing a certain amount of water. More accurate permittivity values of such materials can only be obtained through careful sample preparation and desiccating processes. Ultimately, Martian analogues should be treated in an environment chamber simulating the atmospheric conditions of Mars.

A figure of the conductivity attitude of JSC Mars-1 is demonstrated in Fig. 6. The plotted conductivity values are in range around 10^{-7} S/m which is in good agreement with the results of Simoes et al. (2004) [13]. As mentioned by Simoes the JSC Mars-1 sample shows a highly hygroscopic behaviour which drastically influences the electrical properties. Therefore the small variations of our results to those derived by Simoes et al. (2004) are expected to be due the ambient humidity - for this measurement cycle about 24% - in the laboratory where the presented measurements were performed.

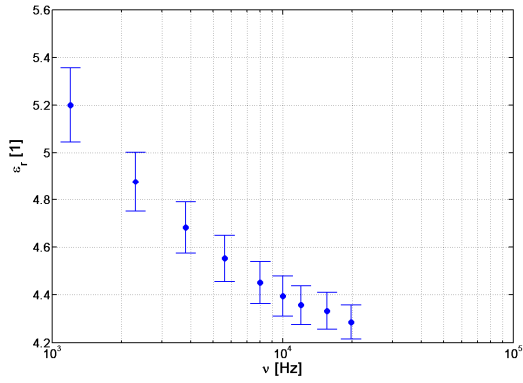


Fig. 5. Evaluated permittivity ϵ_r for Salten Skov.

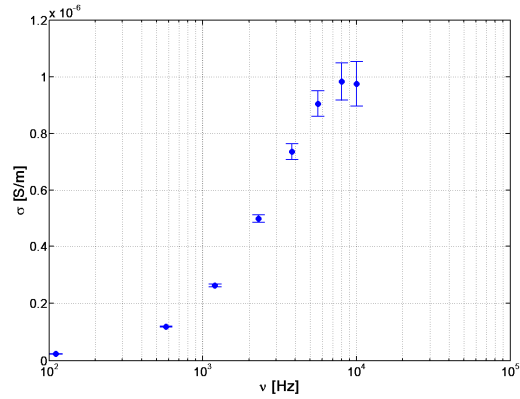


Fig. 6. Conductivity plot of JSC Mars-1.

To test the sensor's ability to detect local inhomogeneities, several measurement-cycles were performed. The set-up for those is shown in Fig.7. The sample is embedded at a well defined position in polystyrol foam. For measurements the layer with the inclusion is covered by another polystyrol layer. PP is then moved laterally to positions ± 30 cm relative to the inclusion centre. The actual sensor position is determined with a linear scale taped on the top layer.



Fig. 7. Measurement set-up for the detection of an inclusion .

Fig. 8 demonstrates the ability to detect local heterogeneities with the PP-sensor. The solid line shows the detected amplitude of the reference signal with no inclusion as a function of the centre-electrode distance to the (assumed) inclusion. Furthermore two measurements with an inclusion are plotted. In every case the signal amplitude shows a minimum, if an inclusion is beneath the sensor. As can be seen in the figure, the signal amplitude exhibits a stronger minimum, if the inclusion is closer to the electrodes. The strongest minimum was detected with a half-sphere (6 cm diameter) filled with granite grains located in 3 cm depth, the smaller one with the same half-sphere with water in 5.5 cm depth, both embedded in polystyrene foam. Beyond the range of the effective depth of investigation z_e , for PP about 2.2 cm (see Sec. 2), a very clear effect for an inclusion is detected too. For high contrast permittivity media laboratory tests showed that the maximum distance of detection for the PP sensor is at about 8 cm depth. This demonstrates the high sensitivity of the HP³-PP instrument. The presented data in Fig. 8 was recorded with a working frequency of 111 Hz, the evaluated errors are in the range of the marker size in the plot. For a detailed understanding of the collected data and the real character of the inclusion in future work theoretical simulations of the signal behaviour are indispensable.

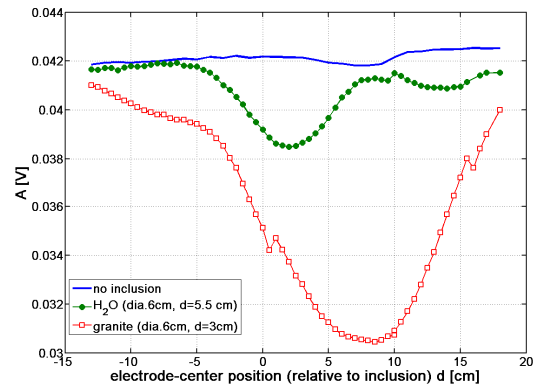


Fig. 8. Signal amplitude for two inclusions as function of electrode centre-position.

Fig. 9 shows the evaluated relative permittivity for 3 classes of glass beads with the diameter of 0.1-0.2 mm (rectangle, solid line), 1-1.25 mm (circle, dotted line) and 3.8-4.3 mm (filled circle, dashed line). The errors of the data point are typically in the size of the plotted symbols. In case of the samples with the lowest diameter significant high permittivity values were detected, which are an indicator for a substantial amount of water in the sample. The glass samples were stored in ambient room conditions, humidity from the air was adsorbed especially on the small grain sizes,

this behaviour demonstrates PP's sensitivity to water traces in the sample.

In Fig. 10 the ability to give an estimation of density variations in the investigated medium is demonstrated. Three glass bead-samples with identical chemical composition show - as expected - a significant increase of the evaluated relative permittivity with increasing bulk density. A direct comparison to e.g. the density-permittivity relation derived by Olhoeft and Strangway (1975) [5] seems not to be reasonable because it was derived for lunar soil samples and a higher frequency range. To give absolute density estimations with PP further measurements in well defined media will have to be performed.

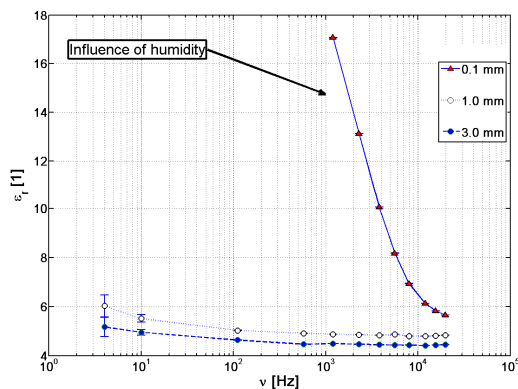


Fig. 9. Relative permittivity ϵ_r for various glass beads.

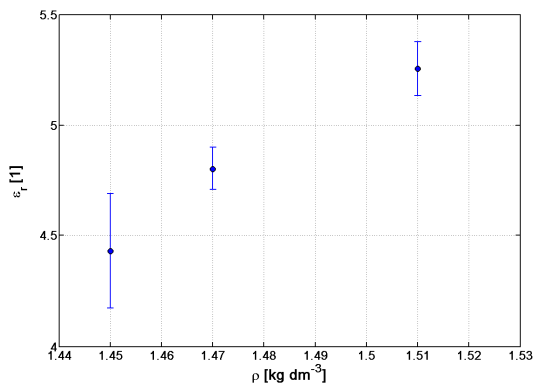


Fig. 10. Glass bead Permittivity ϵ_r , as function of bulk density with a working frequency of 15.6 kHz.

4. CONCLUSIONS

It has been demonstrated through laboratory tests that the developed Permittivity Probe is able to determine the electrical parameters relative permittivity ϵ_r , conductivity σ and the dielectric loss tangent δ of its ambient medium with an error of less than 10 %, which will be reduced to about 5 % after the final calibration.

Textural parameters like local inhomogeneities can be resolved by the permittivity sensor significantly beyond its effective depth of investigation. For high contrast permittivity media a detection distance of about 8 cm was achieved. Furthermore PP is able to estimate density variations in a relative homogeneous medium. Densities could possibly be derived with additional laboratory studies with well known samples and theoretical simulations. In general theoretical simulations in future work are essential for a clear evaluation of the collected data.

5. REFERENCES

1. Wenner F., A method of measuring earth resistivity, *US Bureau of Standards Bulletin*, 12, Sci. paper 259, p 469, 1915.
2. Trautner R. et al., A new instrument for measuring the low frequency electrical properties of planetary subsurface materials, *Proceedings of 37th ESLAB Symposium*, ESA SP-543, 193-196, 2004.
3. Edwards L.S., A modified pseudosection for resistivity and IP, *Geophysics*, Vol.42, 1020-1036, 1977.
4. Loke M.H., Tutorial: 2-D and 3-D electrical imaging surveys (tbc)
5. Olhoeft G.R. and Strangway D.W., Dielectric properties of the first 100 meters of the moon, *Earth and Planetary Science Letters*, 24, 394-404, 1975
6. Mavko G., Mukerji T. and Dvorkin J., *The Rock Physics Handbook*, Cambridge University Press, 1998.
7. Chelidze T.L. and Gueguen Y., Electrical spectroscopy of porous rocks : a review-I. Theoretical models, *Geophys. J. Int.*, 137, 1-15, 1999.
8. Grard R., A quadrupolar array for measuring the complex permittivity of the ground : application to earth prospection and planetary exploration, *Meas. Sci. Technol.*, 1, 295-301, 1990.
9. Hamelin M. et al. , Conductivity and dielectric characteristics of planetary surfaces measured with mutual impedance probes. From Huygens and Rosetta lander to Netlanders and future missions, *Proceedings of 37th ESLAB Symposium*, ESA SP-543, 2004.
10. Grard R. et al., Electric properties and related physical characteristics of the atmosphere and surface of Titan, *Planetary and Space Science*, 54, 1124-1136, 2006.
11. Adiyodi A.K. et al., Dielectric and microhardness studies of methylene blue doped PMMA matrix, *Materials Science-Poland*, Vol. 27, No.1, 2009.
12. Olhoeft G.R., Electrical properties of rocks, in *Physical Properties of Rocks and Minerals*, McGraw-Hill, 257-330, 1981.
13. Simoes F., Laboratory measurements on Martian soil stimulant JSC Mars-1 supporting the calibration of instruments for planetary missions, *Proceedings of 37th ESLAB Symposium*, ESA SP-543, 2004.